

A massive exoplanet candidate around KOI-13: Independent confirmation by ellipsoidal variations

D. Mislis^{1*}, S. Hodgkin¹

¹*Institute of Astronomy, Madingley Road, Cambridge CB3 0HA, UK*

Accepted : 2012 February 08

ABSTRACT

We present an analysis of the KOI-13.01 candidate exoplanet system included in the September 2011 Kepler data release. The host star is a known and relatively bright ($m_{\text{KP}} = 9.95$) visual binary with a separation significantly smaller (0.8 arcsec) than the size of a Kepler pixel (4 arcsec per pixel). The Kepler light curve shows both primary and secondary eclipses, as well as significant out-of-eclipse light curve variations. We confirm that the transit occurs round the brighter of the two stars. We model the relative contributions from (i) thermal emission from the companion, (ii) planetary reflected light, (iii) doppler beaming, and (iv) ellipsoidal variations in the host-star arising from the tidal distortion of the host star by its companion. Our analysis, based on the light curve alone, enables us to constrain the mass of the KOI-13.01 companion to be $M_{\text{C}} = 8.3 \pm 1.25 M_{\text{J}}$ and thus demonstrates that the transiting companion is a planet (rather than a brown dwarf which was recently proposed by Szabo (2011)). The high temperature of the host star (Spectral Type A5-7V, $T_{\text{eff}} = 8511 - 8020$ K), combined with the proximity of its companion KOI-13.01, may make it one of the hottest exoplanets known, with a detectable thermal contribution to the light curve even in the Kepler optical passband. However, the single passband of the Kepler light curve does not enable us to unambiguously distinguish between the thermal and reflected components of the planetary emission. Infrared observations may help to break the degeneracy, while radial velocity follow-up with $\sigma \sim 100$ m s⁻¹ precision should confirm the mass of the planet.

Key words: KOI13 - Kepler mission - Extrasolar planets – transits – thermal emission – ellipsoidal variations – reflected light.

1 INTRODUCTION

In Mislis et al. (2011) we demonstrated the potential for estimating planetary masses solely from light curve (LC) data for a restricted sample of systems. The distinguishing characteristic of these systems is that the planet must be both massive enough and close enough to the host star to induce significant tidal distortions in the stellar ellipsoid. Such non-sphericity in the plane of the sky for a rotating star will lead to a periodic photometric signal which is detectable given sufficient signal-to-noise. In Mislis et al. (2011) we applied the technique to the transiting exoplanet HAT-P-7 observed with Kepler, and estimated the mass of the planet to be $M_{\text{p}}(\text{LC}) = 1.27 \pm 0.12 M_{\text{J}}$ which is very close to the RV solution, $M_{\text{p}}(\text{RV}) = 1.20 \pm 0.05$ (Welsh et al. 2010).

The second exoplanet candidate list released by the Kepler team in February 2011, and published in (Borucki 2011), contains 1235 exoplanet candidates. The light curves span measurements taken between May 2009 and September 2011. Motivated by our previous work, we searched the light curves of all 1235 planetary candidates for evidence of ellipsoidal variation. The brightest and

best candidate for a star showing strong out-of-eclipse ellipsoidal variations is KOI-13.01¹ candidate, which is identified with an A5-7V type star (with a close companion 0.8 arcseconds to the west²). The light curve magnitude is $m_{\text{KP}} = 9.95$ (Kepler passband), and shows primary and secondary eclipses with a published period of 1.7635892 days. The shape of the eclipses are indicative of either a small transiting companion, or a blended system, whereby a deeper eclipse is diluted by contaminating light from nearby stars in the same Kepler pixels.

KOI-13.01 is already the subject of a through analysis of the source characteristics and the transit shape by Szabo et al. (2011). They conclude that the system comprises a double A-star wide binary system, the more massive component of which is being eclipsed by a brown-dwarf or very-low-mass star on the basis of a radius determination $R_{\text{C}} = 2.2 \pm 0.3 R_{\text{J}}$ (R_{C} : companion radius). In this paper we independently confirm that the brighter component of the visual binary is the host star for the eclipses (Section 2).

¹ Shortly before submission of this manuscript we became aware of an analysis of the same system, drawing similar conclusions, submitted by Mazeh et al. (2011arXiv1110.3512).

² Szabo et al. 2011

* E-mail: misldim@ast.cam.ac.uk

2 D. Mislis

Barnes et al. (2011) use a more sophisticated analysis to measure the radius of the host star and transiting companion, including the effects of a gravity-darkened rapidly-rotating host star. The updated values ($R_C = 1.4 \pm 0.016 R_J$, $R_* = 1.77 \pm 0.014 R_\odot$) are significantly smaller than those found by Szabo et al. 2011, and lead Barnes et al. (2011) to conclude that KOI-13.01 may be a planet. Finally, Rowe et al. (2011) presented the system at the 2011 AAS meeting and also suggested the companion is a planet.

In Section 3 we perform modeling of the out-of-eclipse photometric variation, which puts very strong constraints on the mass of the eclipsing/transiting companion, and lends support to the argument that KOI13.01 has a planetary mass.

2 KEPLER DATA

We have used the Kepler public light curve and centroid curve data available from the Kepler archive hosted by the Multimission Archive at STScI (MAST)³ for our analysis. The observations comprised four long-cadence and four short-cadence datasets (spanning Kepler Q1–Q3). The data were processed by the Pre-Search Data Conditioning (PDC) module (Kepler Data Processing Handbook)⁴. For objects brighter than $m_{KP} = 11.3$ some saturation, and then bleeding, of the CCD pixels will occur. This charge is not lost, and using an appropriately shaped mask will preserve the flux, and maintain precise photometry even for extremely bright sources (Gilliland et al. 2010, 2011). Both short-cadence and long-cadence data are equally affected given that they use the same 6 second exposure. Figure 1 we show the Kepler light curve folded on the period of 1.7635892 days found by Borucki et al. (2011), with phase zero set to be the center of the primary minimum.

2.1 Identification of the companion host star

Borucki et al. (2011) suggest that the source associated with KOI-13 is actually a double star (separation 0.8 arcsec, $\Delta mag = 0.4$). Szabo et al. (2011) show that the Kepler source is coincident with the double star (BD+46 2629A and B, hereafter KOI-13A & KOI-13B), two stars of spectral class A, separated by 1.18 ± 0.02 arcseconds with a magnitude difference of $\Delta mag = 0.20 \pm 0.04$ magnitudes.

Howell et al. (2011) use speckle imaging to find a separation of 1.16 arcseconds and $\Delta mag = 0.85$ at 562nm ($\Delta mag = 1.03$ at 692nm) between the two components. However, this photometric difference between the two stars is in serious disagreement with the Szabo et al. (2011) photometry. Having inspected the Szabo et al. (2011) image, we have opted to adopt their value for the magnitude difference between the two stars in the Kepler bandpass (as do Barnes et al. 2011). We note that this is a V-band measurement, which is not identical to the Kepler passband, but for an A-type star, the differences are small. In our analysis (Section 5) we consider the effects of changing the contribution of this companion star to the Kepler light curve. Based on an unresolved spectrum, and a combination of resolved and unresolved photometry, Szabo et al. use model isochrones to find effective temperatures for the A and B components of $T_{\text{eff}}^A = 8511\text{K}$ (8128–8913K) and $T_{\text{eff}}^B = 8222\text{K}$ (7852–8610K) respectively.

The centroid curves for KOI-13 are shown in the middle panel

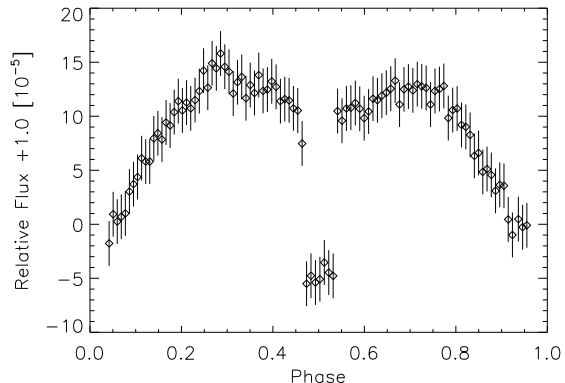


Figure 1. Phase folded light curve and the secondary eclipse of KOI-13 system. The primary transit has been removed to enhance the visibility of the out-of-transit variability.

of Figure 2. Batalha et al. (2010) have demonstrated that the very tiny shifts in centroid, expected for blended occulting sources, can be measured accurately from the Kepler data. Thus they can be used to show where the largest variations in flux are occurring with respect to the center-of-light. The strong periodic offset in the Kepler centroid curve data agrees extremely well with the time of primary transit. Figure 2 (bottom) also shows an illustration of the direction (and magnified amplitude) of the source centroid during primary eclipse. This can be explained simply, if KOI-13A becomes fainter during every transit and the center-of-light moves towards the west (towards KOI-13B). This interpretation independently confirms the conclusions from Szabo et al. (2011) who used both the Kepler pixel light curves, and additional ground-based lucky imaging. Thus we confirm that KOI-13A is the host to the companion.

2.2 Removal of the blended light

For our analysis, the Q1, Q2 and Q3 datasets were used, corresponding to a light curve spanning 418 days in total. The light curve was first corrected to remove the flux from the secondary which we assume to be constant. A magnitude difference of $\Delta mag = 0.2$ was used, and 45 % of the total flux is subtracted from the Kepler light curve (Szabo 2011).

The light curve was phase-folded on the best-fit Kepler period of $P=1.7635892$ (Borucki 2011), rebinned by a factor 1770, and phase=0 set to be the midpoint of the primary transit. We use the updated values for R_C , R_* , α (semi-major axis of the orbit) and inclination (i) from Barnes et al. 2011 ($R_* = 1.76 \pm 0.014 R_\odot$, $R_C = 1.4 \pm 0.014 R_J$, $\alpha = 0.0367$ AU & $i=85.9$). The phase-folded light curve, including the secondary eclipse (but excluding the primary transit to emphasize the out-of-eclipse variation), is shown in Fig. 1. Finally we found no evidence for additional periods in the Kepler corrected light curve, such as Mazeh et al. 2011 suggested ($P = 1.0595$ days).

3 MODELING

In our modeling, we consider four main components which contribute to the out-of-eclipse phase dependence of the light curve of KOI-13, summarised in Equation 1.

³ <http://archive.stsci.edu>

⁴ available via <http://keplergo.arc.nasa.gov/Documentation.shtml>

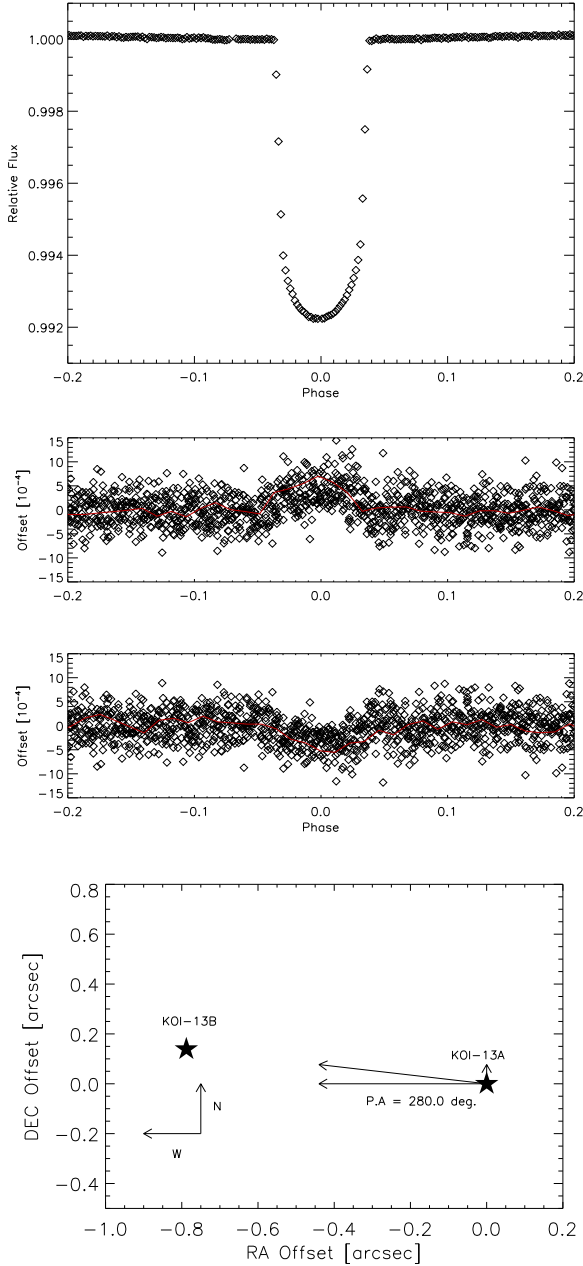


Figure 2. Top: The transit phase folded light curve. **Middle:** X & Y axis offset of the centroid. The offset is periodic (same period as the transit) in the same phase. Offset variations show that the primary star becomes fainter during each transit event. **Bottom:** RA & Dec coordinates of the KOI-13A (right) and KOI-13B (left) plus the RA & Dec offset vectors. The (0,0) point refers to the KOI-13A coordinates ($RA = 286.971^\circ$ & $Dec = 46.8684^\circ$). The vectors have been magnified by a factor of 100.

$$\frac{f_{tot}}{f_\star} = 1 + \frac{f_{th,day} + f_{th,night} + f_{ref} + f_{ell} + f_{dop}}{f_\star} \quad (1)$$

In our simple model we include (1) thermal emission from the companion (day and night side - $f_{th,day}$, $f_{th,night}$), (2) reflected light from the surface of the companion, (3) ellipsoidal variations due to tidal forces between the unseen companion and the star, and (4) flux variations arising from the Doppler shift (Doppler boosting) of the

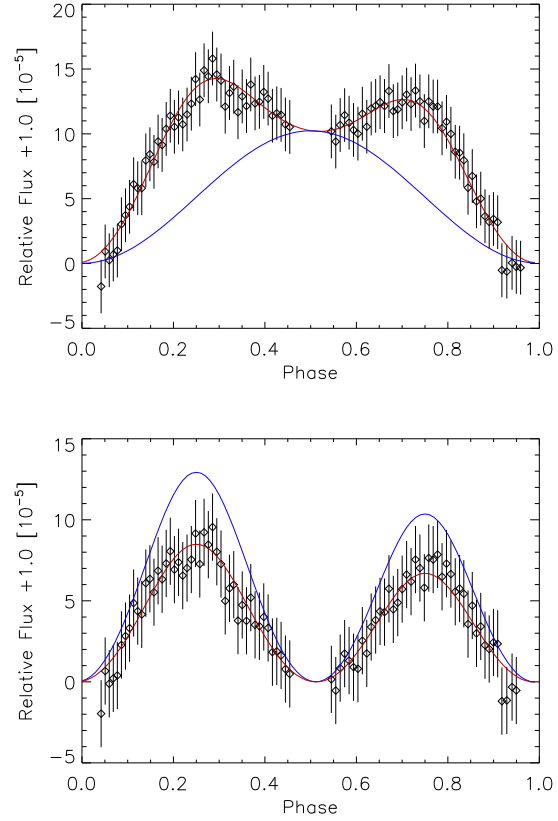


Figure 3. Top: Phase folded light curve and the best fit model (*model - 3*) including all three components (f_{th} , f_{ref} , f_{ell} , f_{dop}). The blue solid line refers to the $f_{th} + f_{ref}$ component. The additional flux from ellipsoidal variations at phase $a = 0.5$ is zero, that's why the total flux at the same phase becomes only from the $f_{th} + f_{ref}$ component (ignoring the secondary eclipse). **Bottom:** The ellipsoidal variation residuals and the best fit (red solid line). The mass of the body which causes these variations must be $M_C \sim 8.3 M_J$. The blue solid line refers to a brown dwarf (BD) ellipsoidal model with mass $M_{BD} = 13.0 M_J$.

stellar spectral energy distribution with respect to the bandpass of the instrument (Loeb & Gaudi 2003, Mazeh & Faigler 2010). This final component contains no additional parameters. The first four components are shown in equations 2–5 (for their derivation, and a detailed discussion, see Mislis et al. (2011)). In Mislis et al. (2011), we show that if we can disentangle the ellipsoidal variations from the close companion's thermal and reflected light components, we can solve for the mass of the companion.

$$\frac{f_{th}(\theta)}{f_\star} = A(\theta) \left(\frac{R_C}{R_\star} \right)^2 \cdot Const \quad (2)$$

$$\frac{f_{ref}(\theta)}{f_\star} = \Phi(\theta) \left(\frac{R_C}{\alpha} \right)^2 \cdot a_g \quad (3)$$

$$\frac{f_{ell}(\theta)}{f_\star} = \beta \frac{M_C}{M_\star} \left(\frac{R_\star}{\alpha} \right)^3 \sin^3(i) \quad (4)$$

$$\frac{f_{dop}(\theta)}{f_\star} = (3 - \rho) \frac{K}{c} \quad (5)$$

4 D. Mislis

where f_{th}/f_{\star} is the relative flux from the thermal emission (for the day side, $f_{\text{th,day}}/f_{\star}$, $A(\theta) = \Phi(\theta)$ and for the night side, $f_{\text{th,night}}/f_{\star}$, $A(\theta) = 1 - \Phi(\theta)$), f_{ref}/f_{\star} is the relative flux from the reflected light, f_{ell}/f_{\star} is the relative flux from the ellipsoidal variations and f_{dop}/f_{\star} is the Doppler Boosting relative flux. $\Phi(\theta)$ is the phase function, α is the semi-major axis, $\text{Const}(T_{\text{eff}}, \lambda, a_{\text{bol}}, \epsilon)$ is a constant function of the effective temperature of the star and the temperature of the planet (Mislis et al. 2011), and β is the gravity darkening. Finally, K is the radial velocity amplitude, ρ is a function of $\rho(\lambda, T_{\text{eff}})$.

$$\rho = \frac{e^{hc/k\lambda T_{\text{eff}}(3 - hc/k\lambda T_{\text{eff}}) - 3}}{e^{hc/k\lambda T_{\text{eff}}} - 1} \quad (6)$$

Our model for the flux changes arising from the ellipsoidal distortion (Eq. 4) is a simple approximation, and assumes that the system is in tidal equilibrium (Rowe et al. 2010, Carter et al. 2011, Mislis et al. 2011). The a_{bol} and ϵ parameters refer to the bolometric albedo and the energy circulation respectively. Both equations 2 & 3 are a function of $\Phi(\theta)$, but the mass of the secondary body is a dependent parameter only in eq. 4 & 5. We note that in our equations the terms R_{\star}/α and R_{C}/α both appear. These are measured directly from the depth and duration of the primary transit and the period of the system. For consistency these values are taken from Barnes et al. 2011.

If we were to solve for and remove the first two components (thermal emission & reflected light), the residual light curve will contain the mass information (Fig. 3 - bottom). An important result of the model is that the ellipsoidal component contributes zero to the total light curve flux (assuming $e=0$) at phase=0.5 (centre of the secondary eclipse), and that the phase function depends only very slightly on the balance between the day- and night-side properties of any companion's emission (i.e. it is extremely difficult to measure this with single passband optical data). Thus the thermal emission and the reflected light components will be very difficult to distinguish in a single filter. Nevertheless, one of the goals of modeling the full Kepler light curve for KOI-13 is to try to constrain the brightness temperature of KOI-13.01. The main difference between our model and other algorithms (such as BEER - Faigler & Mazeh 2011) are that (i) we investigate two phase functions (Lambert and geometrical spheres - Mislis et al. 2011) and (ii) we include distinct reflected and thermal components (including day & night side, a_{bol} , ϵ). The choice of phase functions can alter the mass of the planet by 36% (see Section 5).

KOI-13A is so hot ($T_{\text{eff}} = 8511 \pm 400$ K), and the candidate planet so close ($\alpha = 0.0367$ AU, $\sim 4.5R_{\star}$), that the thermal flux of the candidate is likely to be non-negligible, even at optical wavelengths. The equilibrium temperature for any zero-albedo companion to KOI-13.01 is $T_{\text{eq}} = T_{\text{eff}} \sqrt{R_{\star}/2\alpha} = 2864$ K (for $(R_{\star} = 1.694 \pm 0.013 R_{\odot})$, Barnes et al. 2011), assuming that it does not have its own internal source of heating (as one would expect for a brown dwarf). The hottest known planet discovered to date is probably WASP-33b, with an equilibrium temperature of 2750K, and a brightness temperature of $T_{\text{B}} = 3620^{+200}_{-250}$ K (Smith (2011)), measured from ground-based infrared ($\lambda = 0.9\mu\text{m}$) observations of the secondary eclipse (depth of 0.109 per cent). The relative thermal emission for WASP-33b in the optical (Kepler passband) would be $10^{-4} \times f_{\star}$ (assuming a blackbody). We note that the secondary eclipse of KOI-13.01 is $1.2 \cdot 10^{-4} \times f_{\star}$ (Szabo et al. 2011) in the Kepler passband.

As a starting point, we consider three simple scenarios for the phase light curve data alone, i.e. excluding all datapoints within the primary transit or the secondary eclipse. In case C_{therm} we assume that the bolometric albedo of the companion is fixed at $a_{\text{bol}} = 1.0$,

which means that the planet is perfectly reflective, that the thermal emission of the planet is zero, and therefore the model contains only reflected light and ellipsoidal variations. In case C_{refl} , we assume that the geometric albedo is zero ($a_{\text{g}} = 0.0$), so the reflected light is zero and the model contains only thermal emission ellipsoidal variations, and Doppler boosting (f_{dop} is a function of $\rho(\lambda, T_{\text{eff}})$ and K - Eq. 6). Finally, in case C_{hybr} we consider a hybrid case, and allow a_{g} and a_{bol} to be free parameters, i.e. both thermal emission and reflected light are present in the light curve in addition to any ellipsoidal variations. So in C_{refl} we fit for a_{g} and M_{C} , in C_{therm} we fit a_{bol} , ϵ (energy circulation) and M_{C} , and in C_{hybr} we fit all the parameters above. Eccentricity (e) and the periastron angle (ω) are free parameters in all three scenarios.

As a final step, we add the primary transit and secondary eclipse data back into the light-curve, and re-assess C_{hybr} (and name it C_{hybr}^b), primarily to see if the additional information on the depth of the secondary eclipse can provide useful constraints on the thermal emission from the planet (as has been suggested by Mazeh et al. 2011).

An important and unresolved factor is how we treat the phase function of the reflected light. We consider two approaches: (1) modelling the planet as a Lambert sphere (Russell 1916), assuming that the intensity of the reflected light is $f_{\text{ref}} = 1/\pi$ at phase $z = \pi/2$ (as in the case of Venus); (2) An alternative choice would be to assume that the reflected light is $f_{\text{ref}} = 0.5$ at phase $z = \pi/2$. In Mislis et al. (2011) we demonstrate that this choice leads to a significantly different phase-contribution for the reflected light, and therefore has a significant impact on the derived mass of the companion. The companion mass is significantly larger (by 36 per cent) if we use the Lambert sphere compared to the geometrical sphere. In our analysis we are unable to distinguish between the two cases. Thus, in the next section we present the results from the Lambert sphere case, which gives the larger companion mass.

4 RESULTS

With all three cases we find that the orbit is circular and that the eccentricity value is $e = 0.0 \pm 0.05$. All three scenarios require strong ellipsoidal variations to explain the phase light curve. The hybrid model C_{hybr} is significantly preferred with a confidence of 99 per cent confidence (2.55σ) compared to C_{therm} , and 99.6 per cent (2.85σ) compared to C_{refl} . Scenarios C_{therm} and C_{refl} are indistinguishable at the 1σ level. Table 4 shows the results of all three cases (excluding primary transit and secondary eclipse) and Fig. 3 (top) shows the Kepler light curve and the components for the C_{hybr} scenario. In all three cases, we agree on the mass of the unseen companion to within a few per cent, suggesting that the technique is largely independent of the precise nature (be it thermal or reflected) of the emission arising from the companion. Although note that the mass constraint improves as the model becomes more complex. Both C_{therm} and C_{refl} are significantly less good than the hybrid model, suggesting that components of both thermal and reflected light are contributing to the phase light curve. Note that we do not give errors on ϵ , a_{bol} and a_{g} in C_{hybr} because they are essentially unconstrained at the $1-\sigma$ level, with large degeneracies between a_{g} , a_{bol} , and ϵ .

The mass derived from the best fitting model of the candidate is $M_{\text{C}} = 8.3 \pm 0.9 M_{\text{J}}$, rather more massive than a typical hot Jupiter, but significantly below the brown dwarf or M dwarf mass proposed by Szabo et al. (2011). This error on M_{C} is the error from fitting the model, and does not allow for the uncertainty in the mass of

	C_{refl} [Reflected]	C_{therm} [Thermal]	C_{hybr} [Mixed]
M_C [M_J]	8.0 ± 1.1	8.3 ± 1.0	8.3 ± 0.9
ϵ		0.17 ± 0.17	0.10
a_{bol}		0.01 ± 0.1	0.80
a_g	0.28 ± 0.1		0.28 ± 0.28
e [deg]	0.0 ± 0.05	0.0 ± 0.05	0.0 ± 0.05
χ^2_v	1.042	1.032	1.03

Table 1. Model results for the three main scenarios discussed in the text. From left-to-right the models increase in complexity. We list the fitted parameters and their $1\text{-}\sigma$ errors. In each case we are fitting 90 datapoints in the phase-folded light curve. For scenario C_{hybr} , the parameters shown without errors are essentially unconstrained by the data.

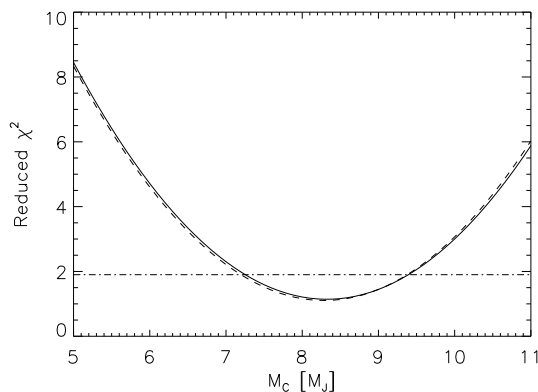


Figure 4. χ^2_v vs M_C for model fits with and without the secondary eclipse (C_{hybr} , C_{hybr}^b) (solid and dashed curves respectively). The horizontal line illustrates the $1\text{-}\sigma$ error level for each model.

the primary, rather this should be seen as a 20 per cent error on the mass ratio, $M_C/M_* = 0.0039$. We take the mass from Szabo et al. (2011) to be $2.05M_\odot$ and assume an error of 10 per cent. We also consider a 0.1 per cent error in the radius ratio R_C/R_* (Barnes et al. 2011). Accounting for both of these leads to a final constraint on the mass of KOI-13.01, $M_C = 8.3 \pm 1.25M_J$.

4.1 How hot is KOI-13.01?

Any attempt to constrain the brightness temperature of the companion is severely hampered by the problem of distinguishing between the reflected and thermal components of our model, exacerbated by the single passband. In principle, if there were no reflected light, nor ellipsoidal variations, we could use the difference between the depth of the secondary eclipse (star only) and the point just before ingress to (or after egress from) the primary transit (i.e. star plus planet night-side) for an orbit with zero eccentricity (e.g. TrES-2, O’Donovan (2010)). In practice, this is rather more complicated, because very small contributions from the ellipsoidal variations, and the marginally visible reflected light components are contributing to the total light of the system at this point in phase. And they need to be included in the modelling to constrain the night-side contribution to the system flux. Mazeh et al. (2011) have ignored these effects, and estimate the temperature of the companion to be 2600K. Our rather more complete treatment of the light curve includes both thermal and reflected components, and includes the secondary eclipse in a self-consistent manner.

This then is our motivation for scenario C_{hybr}^b introduced in the previous Section. We added back into the light curve an additional 36 (in eclipse) data points, while adding no additional parameters to the model, i.e. the shape of the secondary eclipse is completely described by C_{hybr} . A little surprisingly, the additional data do nothing to improve our constraints on the nature of the secondary as parameterized by a_g , a_{bol} and ϵ . Perhaps this should not be so surprising, the depth of the secondary eclipse in a single filter is unlikely to tell us very much about the ratio of thermal to reflected emission from the planets atmosphere. Infrared measurements could perhaps make a significant impact here, as they could be combined with the optical passband to shed light on the colour of the planet. We also note that our solution to the mass of KOI-13.01 is not affected by the additional data points (see Figure 4).

5 DISCUSSION

The very small amplitude of the ellipsoidal variations ($\sim 7.2 \cdot 10^{-5}$) for this period, can only be explained by a body of planetary mass. Increasing the mass of the companion would significantly affect the amplitude of the ellipsoidal variations (Fig. 3 - bottom), therefore we are confident that the mass of the companion KOI-13.01 is $8.3 \pm 1.25 M_J$ (i.e a 1σ upper limit of $9.55M_J$), assuming that there are no other contributions to the Kepler light curve that have so far been ignored in our analysis. It is worth noting that the ellipsoidal component of the light curve is visibly non-symmetric about phase 0.5 due to Doppler Beaming (Figure 3). The difference in heights is $\sim 4.3 \cdot 10^{-6}$, i.e. 3 per cent of the total phase function signal (assuming a simple model which neglects reddening). The mass we derive for the unseen companion to KOI-13A, places the object below the minimum mass for deuterium burning (Spiegel et al. 2011).

One possible source of error in our estimation of the companion’s mass, is the uncertainty in the contribution of the companion A-star to the total Kepler light curve. If we increase the contribution from the nearby stellar component, and the flux we attribute to KOI-13A itself decreases, the mass of the planet becomes correspondingly larger, as the relative contribution of the ellipsoidal variations goes up. However, the effect is rather small when compared to our other sources of error. Specifically, a factor of ± 0.2 magnitudes, leads to a change in the mass of $\pm 0.05M_J$ for the companion. If the Howell et al. (2011) delta-magnitude is used, then the mass of KOI-13b will decrease by ~ 20 per cent; this implies the body is even more planet-like.

Another possible source of error in our treatment of the system is our assumption that the companion behaves as a Lambert sphere. If the correct phase function should be represented by a geometrical sphere, then the best-fit mass of the system will actually be significantly reduced by a systematic factor of 36 per cent, down to $M_C = 5.3M_J$. See Mislis et al. (2011) for a more thorough discussion of this issue. For this paper, we are using the Lambert sphere phase function, which gives the maximum M_C .

The only real way to increase the mass of the unseen companion into the brown-dwarf or stellar regime, is to add yet another unresolved (in the Szabo et al. 2011 lucky imaging), and comparably bright, companion to the Kepler light curve. This seems unlikely, given that the spectral analysis of Szabo et al. (2011) is consistent with the photometry and the model isochrones. Ultimately, the mass of KOI-13.01 can only be fully determined with high spatial resolution (to resolve the components A and B), time-resolved spectroscopy. We estimate that the radial-velocity amplitude for the KOI-13A system will be $K \sim 870 \text{ m s}^{-1}$ for our best-fit mass.

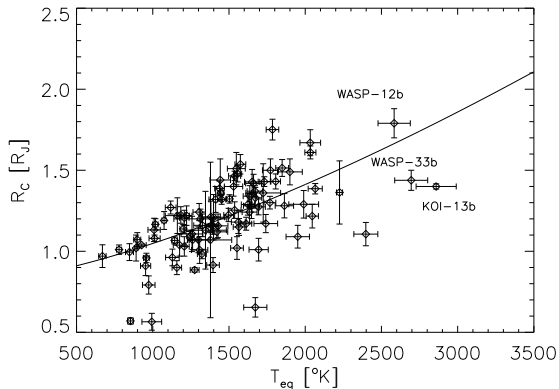


Figure 5. T_{eq} vs R_C for planets found on exoplanet.org. KOI-13.01 is in the middle right part of the plot. The solid line is the $R_C \propto T_{eq}^{1.4}$ model from Laughlin et al. (2011). For the plot we have used exoplanets.org (<http://exoplanets.org/>).

Although measuring precise radial-velocities for a rapidly rotating and spatially-blended A-star is not simple, the formula in Battaglia et al. (2008) suggest that it should be eminently achievable, even with a small telescope, given sufficient signal-to-noise. Ignoring the complications arising from disentangling the two spectra, we find that a signal-to-noise ratio of 10,000 per resolution element, should enable us to reach a velocity precision of around 100 metre/second.

The low amplitude of the ellipsoidal variations rules out the suggestion from Szabo (2011) that the companion could be an M star (Fig. 3). Therefore KOI-13.01 is an exoplanet, and it is now illustrative to consider the object in the light of other exoplanets, especially perhaps WASP-33b which also orbits an A-star. In the T_{eq} vs R_C diagram (Fig. 5), we see that the current radius (Barnes et al. 2011) is in good agreement with the T_{eq} . Laughlin et al. (2011) examine the radius anomaly of exoplanets around their best fit $R \propto T_{eq}^\gamma$ (with $\gamma = 1.4$) relation, and we note that KOI-13.01, as a candidate for one the hottest planets known, may provide a useful constraint on our understanding of planetary structures and atmospheres.

Mazeh et al. (2011) find a mass of 4 ± 2 and $6 \pm 3 M_J$ based on ellipsoidal variations and Doppler beaming effect using R_C , R_* from Szabo et al. 2011. These values have since been updated by Barnes et al. (2011). In our analysis we found that the companion is significantly heavier, smaller and closer to the star, than the Mazeh et al. 2011 measurement. Also, Shporer et al. (2011) found $M_C \sin(i) = 9.2 \pm 1.1 M_J$ based solely on the Doppler beaming effect (also using the Szabo et al. 2011 mass). The Doppler beaming signature in the light curve is roughly an order of magnitude smaller than the ellipsoidal variation, as Shporer et al. (2011) show in their paper. Assuming an inclination of $i=85.9$, the planetary mass from Shporer et al. is $8.1 \leq M_C \leq 10.3$. This mass value is significantly heavier than the Mazeh et al. value (both teams are using the same algorithm and the same system parameters), but agrees with our mass value.

6 CONCLUSIONS

We present modeling of the KOI-13.01 Kepler light curve, confirming the planetary nature of the companion. Our analysis illustrates

the wealth of information that can be extracted from high precision light curves, in the absence of spectroscopy. We find that the out-of-eclipse light curve of KOI-13.01 is dominated by two effects. The light contributed by the planet is at the same amplitude as the ellipsoidal variations induced in the star.

We are unable to solve for the relative contributions of thermal and reflected emission from the planet, however we expect the planet to be one of the hottest known, given its close proximity to an A-star, and its large radius. The equilibrium temperature for any zero-albedo companion to KOI-13.01 is $T_{eq} = T_{eff} \sqrt{R_*/2a} = 2864\text{K}$, which is rather hotter than calculated for WASP-33b and WASP-12b. We suggest that infrared observations would help to disentangle the thermal and reflected components of the light curve.

By modelling the light curve, we find that the mass of the planet is $M_C = 8.3 \pm 1.25 M_J$, robust against any assumptions about the albedo of the planet. We also find that the planet is orbiting in a circular orbit ($e = 0.0 \pm 0.05$). Our results suggest that the density of the planet is ~ 3 times larger than Jupiter's density. This value is not surprising. There are much more dense exoplanets, such as XO-3b (density ~ 6.5 times more dense than Jupiter - exoplanet.org)

We have studied the case that the system is an M-dwarf or brown-dwarf eclipsing companion, but neither of these solutions can explain the light curve we observe. The expected radial velocity amplitude for KOI-13 system is $K \sim 870 \text{ m s}^{-1}$, which will be relatively easy to measure despite the nature of the primary (a rapidly rotating A star) and the contamination from the close A-star companion. It would be an interesting exercise to search all of the Kepler light curves to look for the signature of ellipsoidal variations as a planet detection method, even in the absence of transits.

ACKNOWLEDGMENTS

This research has made use of NASA's Astrophysics Data System Bibliographic Services. DM is supported by RoPACS, a Marie Curie Initial Training Network funded by the European Commissions Seventh Framework Programme.

REFERENCES

- Barnes, W., Linscott, E., and Shporer, A., 2011, ApJ 197, 10B
- Battaglia G., Irwin M., Tolstoy E., Hill V., Helmi A., Letarte B. & Jablonka P., 2008, MNRAS, 383, 183
- Batalha N., Rowe J., Gilliland R. et al. 2010, ApJ 713L 103B
- Borucki W., Koch D., Basri G., et al. 2011, arcXiv 1102, 541B
- Carter J., Rappaport S., & Fabrycky D., 2011, ApJ, 728, 139C
- Cowan N., Agol E., 2011, ApJ 729, 54C
- Croll B., Jayawardhana R., Fortney J., et al. 2010 ApJ 718, 920C
- Gilliland R., Jenkins J., Borucki W., et al. 2010, ApJ, 713, 160G
- Gilliland R., Chaplin W., Dunham E., et al. 2011, ApJ, 197, 6G
- Hansen B.M.S. 2008, ApJS, 179, 484H
- Howell S., Everett M., Sherry W., et al. AJ, 142, 19H
- Laughlin, G., Srismani, M., & Adams, F., ApJL, 729, 7
- Loeb A., Gaudi S., 2003, ApJ 588, 117
- Mislis D., Heller R., Schmitz J, et. al. 2012, A&A, 538A, 4M
- O'Donovan F. T., Charbonneau D., Harrington J., et al. 2010, ApJ, 710, 1551O
- Rowe J., Borucki W., Koch, D., et al. 2010, ApJ, 713L, 150R
- Rowe J., Borucki W., Howell, S., et al. 2011, AAS, 21710304R
- Smith A., Anderson D., Skillen I., et al. 2011, MNRAS 416, 2096S145W

Shporer A., Jenkins J., Rowe J., et al. 2011, AJ, 142, 195S
Spiegel D., Burrows A., Milsom J., 2011, ApJ 727, 57S
Szabo M., Szabo R., Benko M., et al. 2011, arXiv:1105.2524v1
Welsh W., Orosz J., Seager S., et al. 2010, ApJ 713, 145W

This paper has been typeset from a $\text{T}_{\text{E}}\text{X}/\text{L}_{\text{A}}\text{T}_{\text{E}}\text{X}$ file prepared by the author.